# Effect of Rare-Earth Component of the RE/Ni Catalyst on the Formation and Nanostructure of Single-Walled Carbon Nanotubes

**Mingguang Yao, Bingbing Liu,* Yonggang Zou, Lin Wang, Tian Cui, and Guangtian Zou**

*National Lab of Superhard Materials, Jilin University, Changchun 130012, China*

**Jixue Li**

*State Key Laboratory of Inorganic Synthesis and Preparative Chemistry, Jilin University*

**B. Sundqvist**

*Department of Physics, Umeå University, 90187 Umeå, Sweden*

*Received: February 14, 2006; In Final Form: June 14, 2006*

A systematic experimental study has been carried out on the efficiency of bimetallic catalysts based on Ni and the rare-earth elements Y, La, Ce, Nd, Gd, Tb, Dy, Ho, Er, and Lu (group A) and Eu, Sm, Yb, and Tm (group B) in the synthesis of single-walled carbon nanotubes (SWNTs). The two groups give quite different results when analyzed by a combination of SEM/TEM and Raman and UV−NIR spectroscopies. The elements in group A have an obvious catalytic effect and increase the yield of SWNTs dramatically, whereas those in group B are not efficient catalysts. The diameter distribution of the synthesized SWNTs was also affected by the rare-earth element used. For group A metals, there is a tendency that the fraction of small-diameter tubes decreases with decreasing ionic radius of the rare-earth element used. EDX and X-ray analyses indicate that group A metals deposit on the cathode deposits and form rare-earth carbides, whereas no group B metals are found in cathode deposits, except for a small amount of Tm present in the form of thulium carbide. Further analysis indicates that there is a very strong correlation between the ability to form rare-earth carbides and the catalytic efficiency for the formation of SWNTs.

## Introduction

The unique physics and chemistry of single-walled carbon nanotubes (SWNTs) imply a great potential for SWNTs in nanoscience and in technological applications.[1−4] Such applications require large-scale synthesis of SWNTs with desired nanostructures and with high purity. One of the most widely used methods, the arc discharge method, can produce SWNTs with a high degree of crystallinity and low defect concentration on a large scale.[5,6] One of the most critical parameters in SWNT synthesis is the catalyst used, and bimetallic catalysts have been found to have synergistic effects in the formation of SWNTs, especially when Ni is combined with rare-earth (RE) elements.[6] To date, several rare-earth elements, including Y, Ce, Tb, La, Ho, Gd, and Pr, have been used together with Ni in bimetallic catalysts for the synthesis of SWNTs.[6−12] These works show that the addition of rare-earth elements into the catalysts often greatly improves the yield of SWNTs and even influences the nanostructure of the SWNTs, such as diameter and helicity. Regarding the respective roles of the metals in the bimetallic catalyst for the growth of the SWNTs, some suggestions have been made. Early studies indicated that Y was separated from Ni and that only Ni catalyzed the growth of SWNTs when Y/Ni was used.[10] Recently, HRTEM studies by Gavillet et al. revealed that several atomic layers of rare-earth carbide were frequently found on catalyst nanoparticles directly associated with the roots of SWNTs bundles, when they used RE/Ni (RE = Ce, Y, La) as the catalyst.[11] Krestinin et al. also suggested that endometallofullerene served as a precursor of a nanotube nucleus for SWNTs when they used RE/Ni catalysts (RE = La, Gd, Ce, Pr).[12] A theoretical simulation by Deng et al. indicated that one metal in a bimetallic catalyst acts as a catalyst for SWNT nucleation and the other promotes growth.[13] However, the exact roles played by catalyst metals in the formation of SWNTs are still uncertain, and further studies are needed to obtain a clear understanding of nanotube growth.

The rare-earth elements, including 14 lanthanide metals, Y, and Sc, have very similar chemical properties because of the very similar electronic configurations of their outermost electrons. However, they also have slight differences. For example, most of them are trivalent, with Eu also having a valence of 2+ and Ce also having a valence of 4+. The ionic radii of rare-earth metals gradually decrease with increasing atomic number, the so-called "lanthanide contraction". There has been no systematic and detailed study on the effects of the series of rare-earth metals as catalysts in the formation of single-walled nanotubes. Whether all rare-earth metals exhibit synergistic effects on the formation of SWNTs and whether the nanostructure of SWNTs can be tuned by adding selected rare-earth metals to Ni for use as bimetallic catalysts are still open questions with great interest and relevance for SWNT science. We therefore decided to add a series of RE elements to nickel and to use these bimetallic compounds as catalysts in a study of the formation of SWNTs, including their catalytic effects on the yield and nanostructure of SWNTs. Such a study might also provide some clues to understand the growth mechanism of the

* Corresponding author. Tel.: +86 431 5168256. Fax: +86 431 5168883. E-mail: liubb@jlu.edu.cn.

10.1021/jp060942b CCC: $33.50 
Published on Web 07/19/2006

SWNTs and the factors that determine the activity of rare-earth metals as catalysts.

In this work, we have carried out a systematic experimental study using a series of rare-earth elements together with Ni as catalysts in the synthesis of SWNTs. The RE elements used were Y, La, Ce, Nd, Sm, Eu, Gd, Tb, Dy, Ho, Er, Tm, Yb, and Lu. We found that these rare-earth metals can be classified into two groups that behave quite differently as catalysts. Group A elements, which includes Y, La, Ce, Nd, Gd, Tb, Dy, Ho, Er, and Lu, have a strong catalytic effect and increase the yield of SWNTs dramatically, whereas those in group B, Eu, Sm, Yb, and Tm, are not effective as catalysts. The diameter distribution of the synthesized SWNTs was also affected by the rare-earth components. Further analysis of the catalyst components indicates that there is a very strong correlation between the tendency to form rare-earth carbides and the catalytic efficiency in the formation of SWNTs.

## Experimental Section

A conventional arc discharge was used for the preparation of SWNTs. The SWNT samples were generated by arcing metal-oxide-impregnated graphite rods in a helium atmosphere at a pressure of 600 Torr. The cathode was a graphite rod with a diameter of 8 mm. Spectrally pure graphite rods, 6 mm in diameter, were drilled; filled with a mixture of rare-earth oxide (99.99%), Ni (99.9%), and graphite; and used as anodes. The metal oxides used in this experiment were $Y_2O_3$, $La_2O_3$, $CeO_2$, $Nd_2O_3$, $Sm_2O_3$, $Eu_2O_3$, $Gd_2O_3$, $Tb_4O_7$, $Dy_2O_3$, $Ho_2O_3$, $Er_2O_3$, $Tm_2O_3$, $Yb_2O_3$, and $Lu_2O_3$. The powder mixtures had a uniform molar ratio of RE/Ni/C = 1:2:97 to facilitate a comparison of the results. For the same reason, we carried out our study with fixed parameters for the operation of the arcing process, with only the anode composition as a variable. The arc discharge was run at a current of ~90 A and a voltage of 25 V. These experimental conditions were optimized for the synthesis of SWNTs with Ho/Ni, Y/Ni, and Ce/Ni catalysts.[7,9]

After the arc discharge, we obtained different products from the two groups of RE/Ni catalysts. In the case of group A RE/Ni catalysts, we could collect a large quantity of SWNT-rich soot, including weblike products, collarlike products on the cathode, and some chamber soot deposited on the inner wall of the reaction chamber. In this group, the catalysts containing Y, Ho, Er, and Tb produced less chamber soot than the others. In the case of the group B RE/Ni catalysts containing Eu, Sm, Yb, and Tm, the products were quite different. Except in the case of Tm, hardly any weblike products were obtained, and only sootlike products were found surrounding the cathode and on the chamber wall after the arc discharge. Even for Tm/Ni, only a small amount of weblike products, much less than for the group A elements, was obtained in addition to the sootlike products. For all catalysts, a hard, black cathode deposit was also collected after the arc discharge.

The as-grown products were collected and characterized using scanning electron microscopy (SEM, JEOL, JSM-6700F); transmission electron microscopy (TEM, JEOL-3010); Raman spectroscopy (Renishaw 1000) using excitation wavelengths of 514.5 nm (argon ion laser), 632 nm (He−Ne laser), and 780 nm (diode laser); X-ray diffraction (XRD, Rigaku, D/max-RA); and UV−NIR spectroscopy (UV-3150, Shimadzu).

## Results and Discussion

Figure 1a shows a typical optical image of the weblike and collarlike products synthesized with a group A RE/Ni catalyst. In general, the weblike product is very sticky and transparent in some regions. The collarlike product around the cathode is free-standing and easy to exfoliate (see inset of Figure 1a). The SWNT content of the weblike and collarlike fraction is higher than that in the chamber fraction, which is consistent with previous studies.[7,9]

Figure 1b shows a typical SEM image of the as-grown SWNT in a thin and transparent region of the weblike product. The inset of Figure 1b shows a typical HRTEM image of a SWNT bundle from such a sample. On the other hand, TEM observations of the products synthesized using RE/Ni catalysts from group B (RE = Eu, Sm, Yb) show very few SWNTs, and these products are dominated by nanoparticles (Figure 1c). A slightly better purity of SWNTs was obtained with Tm/Ni catalyst.

Raman spectroscopy is a very powerful technique for characterizing SWNTs. The two most prominent features observed in the first-order resonant-Raman spectrum of SWNTs are the low-frequency radial breathing mode (RBM) located typically in the range of 100−300 $cm^{-1}$ and the high-frequency G band between 1500 and 1600 $cm^{-1}$, which is composed of several tangential modes due to stretching vibrations of the SWNT sidewall carbon−carbon bonds.[14] In addition, another peak around 1350 $cm^{-1}$, the D band, is associated with SWNT defects and amorphous carbon present as impurities. In general, the ratio between the G and D bands, *G*/*D*, is used to roughly gauge the defects and estimate the purity of the SWNTs.

Figure 2a shows the Raman spectra of the as-grown SWNT samples using a 632-nm excitation wavelength. The spectra can clearly be classified into two groups. The upper part shows the Raman spectra of SWNTs (taken from weblike regions) produced using group A RE/Ni catalysts. The curves are labeled with the RE element used and shown in order of increasing RE ionic radii. The ionic radius of Y is close to those of Dy and Er. The Raman spectra from this group all have the characteristic peaks of SWNTs. The lower part shows the Raman spectra of sootlike deposits produced using group B RE/Ni catalysts. Although these spectra also show the presence of SWNTs, the high relative intensity of the D band indicates that the samples contain relatively fewer SWNTS and a high fraction of amorphous carbon.

As shown in Figure 2b, the measured *G*/*D* values depend strongly on the RE component used in the bimetallic RE/Ni catalysts. Using RE catalyst components from group A results in much higher values for the ratio *G*/*D* than does using elements from group B, indicating that impurity and defect levels in the SWNTs produced are much higher when elements from group B are used.

The RBM frequency ($w$) can be used to determine the diameter $d$ of the SWNTs present in the sample using the equation $d = 224/(w - 14)$.[15] From Figure 2a, we see that the relative intensities and positions of the low-frequency RBM peaks depend on the RE component in the bimetallic RE/Ni catalysts. The RBM peaks in Raman spectra from most group B RE/Ni samples (obtained using Sm, Eu, and Yb) are different from those found for group A RE/Ni samples, but the RBM peaks for the sample obtained using a Tm/Ni catalyst are close to those of group A RE samples. For the spectra from group A samples, the strongest RBM peaks have been normalized to enable convenient comparison of the relative intensities of the RBM peaks. The three dominant peaks at 163, 180, and 189 $cm^{-1}$ obtained for this group of samples correspond to diameters of 1.50, 1.34, and 1.27 nm, respectively. However, the relative intensities of these three RBM peaks vary with the ionic radius of the RE used in the catalyst. The relative intensities of the higher-frequency peaks at 180 and 189 $cm^{-1}$ decreased with

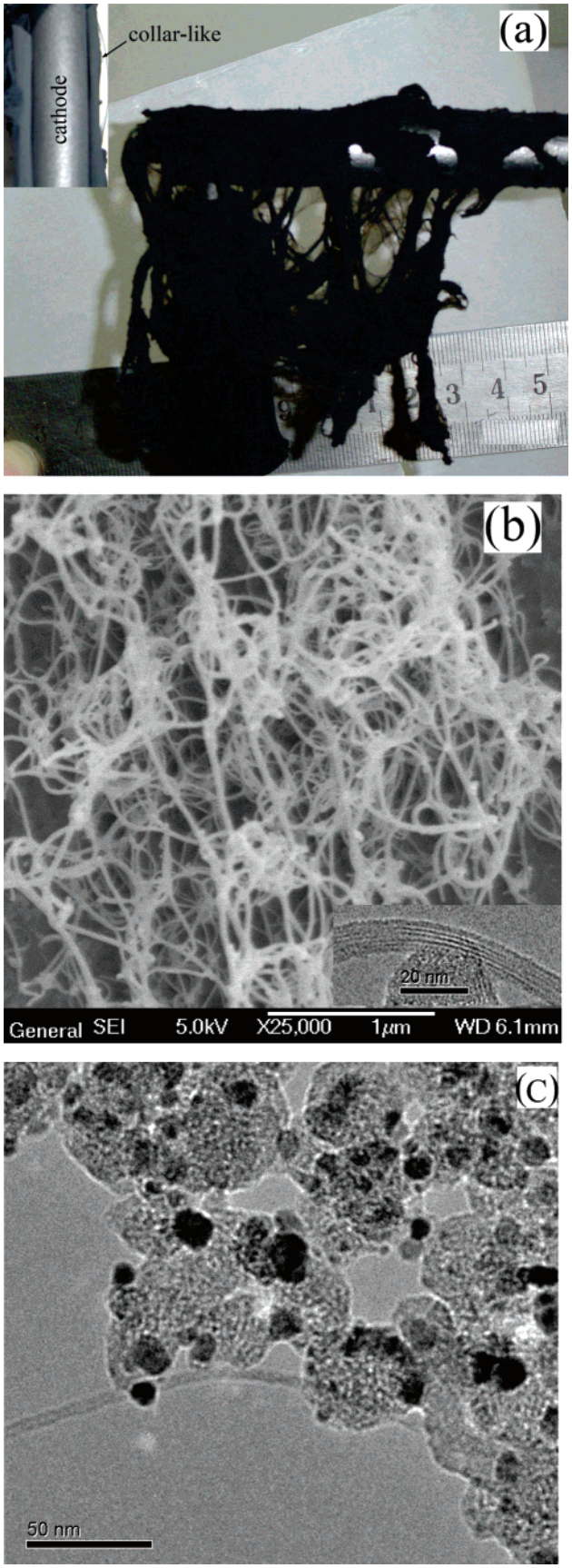


**Figure 1.** (a) Optical image of the weblike product synthesized using group A RE catalysts. The inset shows the collarlike product, free-standing around the cathode. (b) SEM image of as-grown SWNTs synthesized using a group A Re/Ni catalyst (here, the Er/Ni catalyst). The inset shows HRTEM image of a SWNT bundle. (c) TEM image of sootlike deposit obtained using Eu/Ni catalyst.

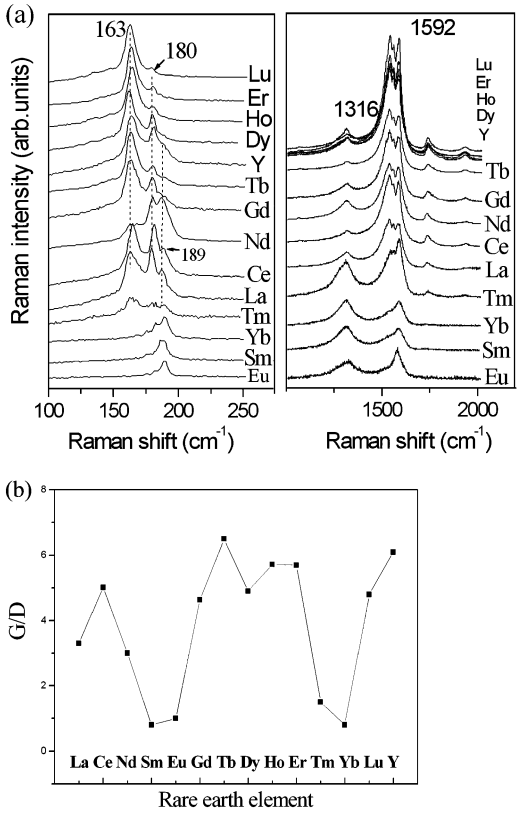


**Figure 2.** (a) Raman spectra of SWNTs obtained using different RE/Ni catalysts. Spectra obtained with a 632-nm wavelength laser. (b) Raman intensity ratios between the peaks at 1316 and 1592 $cm^{-1}$ (*G*/*D*), plotted as a function of the RE metal used in the catalysts.

decreasing ionic radius of the RE used in the catalyst (Figure 2a), indicating that the relative quantity of small-diameter tubes in the samples also decreased with decreasing ionic radius of the RE.

Because SWNT Raman spectra are laser-excitation-selective,[14] two other excitation wavelengths, 514.5 and 780 nm, were employed to further analyze the diameter distribution of the samples. A similar tendency is again found in the Raman spectra for the group A samples. For example, two RBM peaks at around 165 and 183 $cm^{-1}$ were mainly excited in the 514.5-nm-excitation Raman spectra (low-frequency region, Figure 3a). There is a tendency for the relative intensity of the peaks around 165 $cm^{-1}$ to increase and for that of the peaks around 183 $cm^{-1}$ to decrease slightly with decreasing ionic radius of the RE used in the catalysts. For 780-nm-excitation Raman spectra (see Figure 3b), there are RBM peaks at 138, 151, 165, 181, and 202 $cm^{-1}$ for samples produced using a La/Ni catalyst, whereas the high-frequency peak at 202 $cm^{-1}$ can hardly be detected for samples produced using Nd/Ni. For samples produced using the group A RE with the smallest ionic radius, Lu, the peaks at 181 and 202 $cm^{-1}$ disappear, but the peak at 138 $cm^{-1}$ becomes stronger. This result also shows that the relative quantity of small-diameter tubes in the samples decreases with a decrease in the ionic radius of the RE used in the catalysts. Figure 3 also shows Raman spectra with 780-nm excitation for the sootlike products obtained with Tm/Ni, Yb/Ni, and Eu/Ni catalysts. SWNT signals were detected in some regions of these samples. The results indicate that the diameter distribution of SWNTs in these samples is quite different from that in samples produced using group A catalysts, except for Tm/Ni, for which the diameter distribution is similar to that of group A samples.

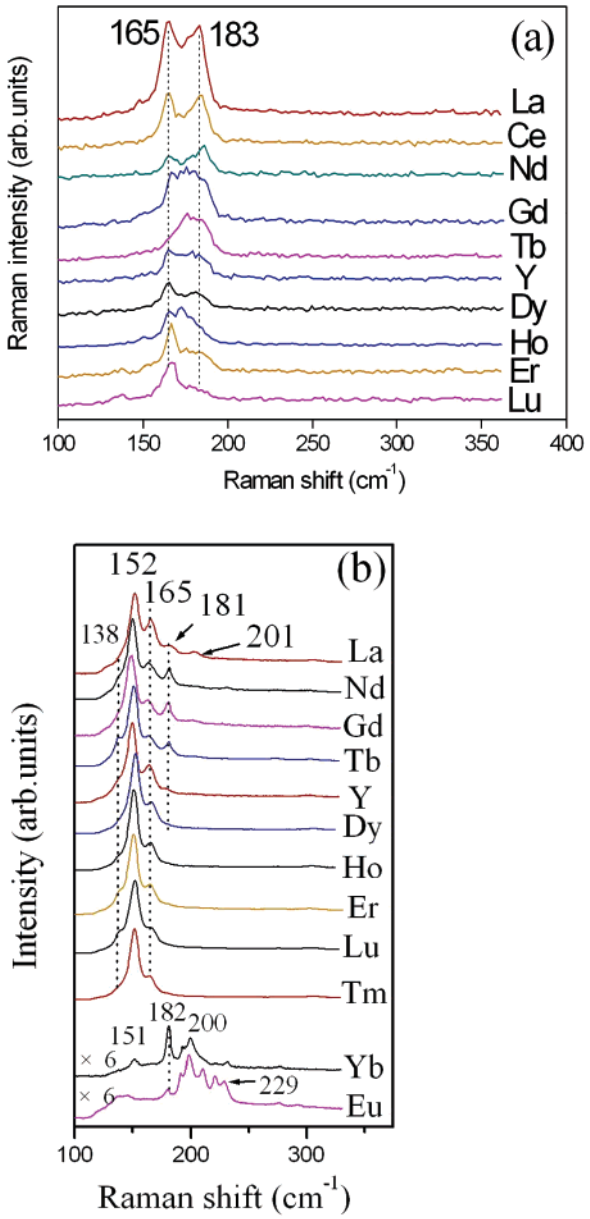


**Figure 3.** RBM region in Raman spectra of SWNTs produced using different RE/Ni catalysts: (a) 514.5-nm excitation, (b) 780-nm excitation.

UV−NIR spectroscopy was used to further evaluate the purity of as-grown SWNT samples synthesized with various RE/Ni catalysts. We followed an experimental procedure described in a very recent article.[5] In brief, the as-grown product (except for the cathode deposit) was mechanically homogenized, and 10 mg of the homogenized sample was dispersed in 20 mL of *N*,*N*-dimethylformamide (DMF) in a ultrasonic bath. After several dilution/ultrasonication cycles, the SWNT/DMF solution was used for UV−NIR absorption measurements. Figure 4 shows the $S_{22}$ (7750−11750 $cm^{-1}$) transition band of the absorption spectra for SWNT samples obtained with different RE/Ni catalysts. The ratio of the spectral area of the $S_{22}$ transition band (top) to the total area under the spectral curve between 7750 and 11750 $cm^{-1}$ is proportional to the purity of SWNT in the samples (see Figure 4a and b). A higher ratio corresponds to higher SWNT purity. To compare the relative purity (RP) of the samples, we define the RP of the as-grown samples as

$$\mathrm{RP} = \frac{S_{22}/S_{\mathrm{total}}}{S_{22(\mathrm{YNi})}/S_{\mathrm{total(YNi)}}}$$

Here, the ratio $S_{22(YNi)}/S_{total(YNi)}$ of samples synthesized using bimetallic Y/Ni catalyst was used as a reference. Figure 4c shows the RPs of samples synthesized using the different RE/Ni catalysts.

From Figure 4c, we can see that the RE component in the catalysts has a dramatic effect on the purity of the as-grown SWNT samples. The RP of the SWNT samples synthesized using group A RE/Ni catalysts is obviously higher than that of the samples synthesized using group B RE/Ni catalysts. The results also indicate that the SWNT content in the samples produced using Tm/Ni is higher than that obtained using the (Sm, Yb, Eu)/Ni catalysts. The samples obtained using Tb, Er, Ho, or Y together with Ni as the catalyst show the highest purity. The large difference between the two groups of RE-element catalysts agrees well with the results of the Raman measurements. In addition, the $S_{22}$ band in the UV−NIR spectra of SWNT samples is useful for the determination of the SWNT diameter distribution.[16,17] It is known that, with increasing SWNT diameter, all interband transition peaks shift to lower energy (i.e., frequency). It is observed that the center of the $S_{22}$ band shifts to lower frequency with decreasing ionic radius of the rare-earth element used in catalysts to synthesize SWNTs for group A RE metals. This shift corresponds to an increase of the mean SWNT diameter. To obtain the fractional abundance of the different diameters more accurately, the $S_{22}$ band was fitted with a Lorentzian shape and then analyzed following a procedure reported in the literature.[17] The resulting data for the diameter distribution are shown in Figure 4d. Again, there is the similar tendency that the relative quantity of small-diameter tubes decreases with a decrease in the ionic radius of the RE used in the catalysts, which is consistent with the results from Raman measurements.

To investigate the roles played by the RE in the synthesis of SWNTs, pure nickel was also employed to synthesize SWNTs for comparison. This gives a very poor purity of SWNTs in the soot. An affirmative finding from these studies is that the addition of group A RE elements to Ni as catalysts significantly increases the yield of SWNTs. To further understand the role of the catalyst in the synthesis process, X-ray diffraction and energy-dispersion X-ray (EDX) analysis were employed to investigate the compositions of the catalysts and their distribution in the product. X-ray measurements were performed under uniform conditions. Figure 5a and b shows the X-ray diffraction diagrams for cathode deposits collected after arcing anodes filled with group A RE/Ni catalysts. In these XRD patterns, we observed signals from both rare-earth carbides and carbonaceous deposits for all RE/Ni catalysts of group A. Note that $CeC_x$ and $TbC_x$ denote cerium carbide and terbium carbide, forming $Ce_2C_3$, $CeC_2$ and $TbC_2$, $TbC_{0.4}$, respectively. Several X-ray diffraction peaks labeled with asterisks in Figure 5a were tentatively assigned to $NiRE_xC_y$ for deposits obtained with La/Ni, Nd/Ni, and Gd/Ni catalysts. However, in most cathode deposits obtained using group B RE/Ni catalysts, we detected only carbonaceous materials. The exception was again the cathode deposit obtained using Tm/Ni (Figure 5a), but the thulium carbide X-ray diffraction signal was weaker than the carbide signals from the group A samples. When we used Ni or Ni/Co as the catalyst to synthesize SWNTs, we also obtained poor yields of SWNTs. X-ray diffraction and EDX analyses of the cathode deposits indicated that catalyst metals or metal carbides were hardly present in the cathode deposits.

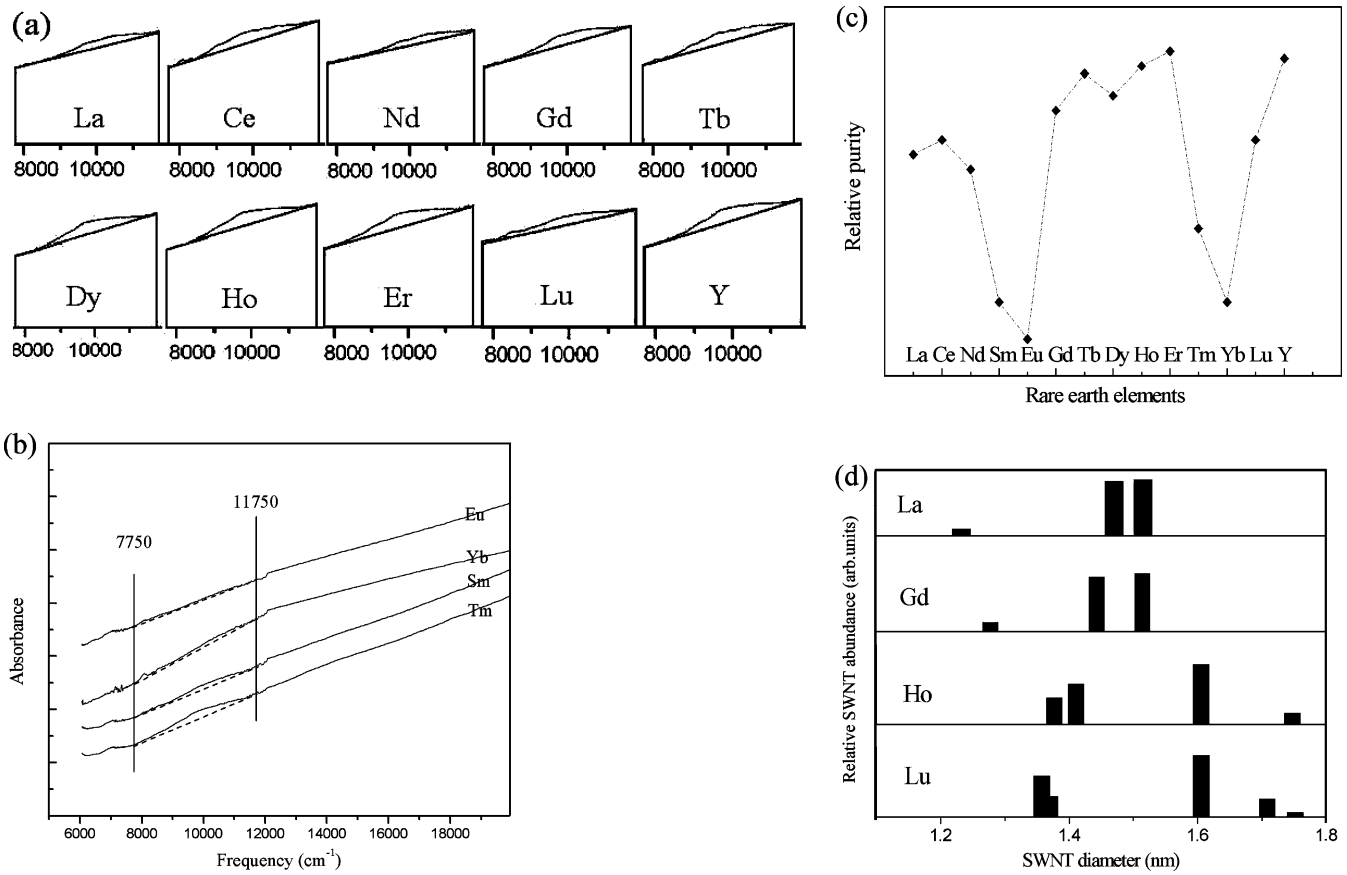


**Figure 4.** Solution-phase NIR spectra of as-grown SWNT samples synthesized using (a) group A RE metals with a constant amount of Ni as catalysts and (b) Eu, Sm, Yb, and Tm with Ni as catalysts. The spectra, offset for clarity, were all obtained at similar SWNT/DMF concentrations. (c) Relative purity (RP) as defined in the text plotted against the RE element used in the bimetallic catalyst. (d) Relative fractional SWNT abundances obtained from optical spectra.

We further used EDX analysis to investigate the catalyst distribution in the cathode deposits and in sootlike samples produced by arcing group B RE/Ni-filled anodes. The results show that the cathode deposits contained almost no RE or Ni, except for the Tm/Ni cathode deposit, which contained a small amount of Tm. The RE and Ni are distributed in the sootlike product, where the ratio between RE and Ni is almost as high as in the initial anode. To investigate whether an excess of Eu (compared to the RE content in the case of group A REs) in the soot suppresses the yield of SWNTs, we also decreased the initial ratio of Eu to Ni in the anode from 1:2 to 0.2:2. After arcing this anode, EDX analysis showed that the obtained sootlike product contained much more Ni than Eu (~10:1). However, the purity of SWNTs was still very low. We further employed HRTEM with EDX to study the compositions of the sootlike products obtained with Eu/Ni (1:2) as the catalyst. HRTEM observations showed that the element Eu was frequently present in the form of Eu−Ni−O compounds and even as uncoated europium oxide nanoparticles (see Figure 6a). HRTEM observations also indicated that the core of the catalyst particle linked with a SWNT bundle is pure crystalline Ni (Figure 6b).

We found that group A RE elements form stable rare-earth carbides whereas group B RE elements, with the exception of Tm, can scarcely form rare-earth carbides under arc conditions. Tm has a higher ability to form a carbide than other RE metal in group B, but its ability is still lower than that of the members of group A. This intermediate carbide-forming ability of Tm correlates with the observation of a higher yield of SWNTs than for other catalysts containing group B RE metals but lower yield than for group A RE catalysts, as identified by Raman and UV studies. Furthermore, the RE metals (Tb, Er, Ho, and Y) that show the best catalytic efficiencies in SWNT synthesis when added to Ni all have strong rare-earth carbide signals. Comparing the catalytic efficiency of RE metals in the synthesis of SWNTs with the ability of RE metals to form rare-earth carbide, there is a strong correlation between the ability of the RE to form a rare-earth carbide and the catalytic efficiency. These results suggest that the ability of RE metals to form rare-earth carbides plays an important role in the formation of SWNTs.

The vapor−liquid−solid (VLS) growth model proposed by Gavillet et al.[11] might be used to explain our results. From HRTEM studies, they observed that the RE component accumulated at the surface of catalyst particles in the form of carbides and that it was directly related to the nucleation of SWNT ropes when they used RE/Ni catalysts. In their experiments, only Y, Ce, and La were studied, and they found that long SWNT ropes were always linked to nanoparticles whose RE/Ni composition ratio was lower than 11 atom %. Our EDX analysis indicates that weblike products containing abundant SWNTs usually contain both Ni and RE and that the average ratio RE/Ni is in the range of 1:5−1:10 for all rare-earth metals from group A. Further, in the case of Ho/Ni catalysts, we studied several catalyst nanoparticles by using an HRTEM instrument equipped with an EDX apparatus and found that long SWNT ropes were generally linked to catalyst nanoparticles whose Ho/Ni composition ratio was small (in agreement with Gavillet's observation). We thus believe that this growth model might be valid for all RE/Ni catalysts, and from this model, we can further understand that the inefficiency of group B RE metals in

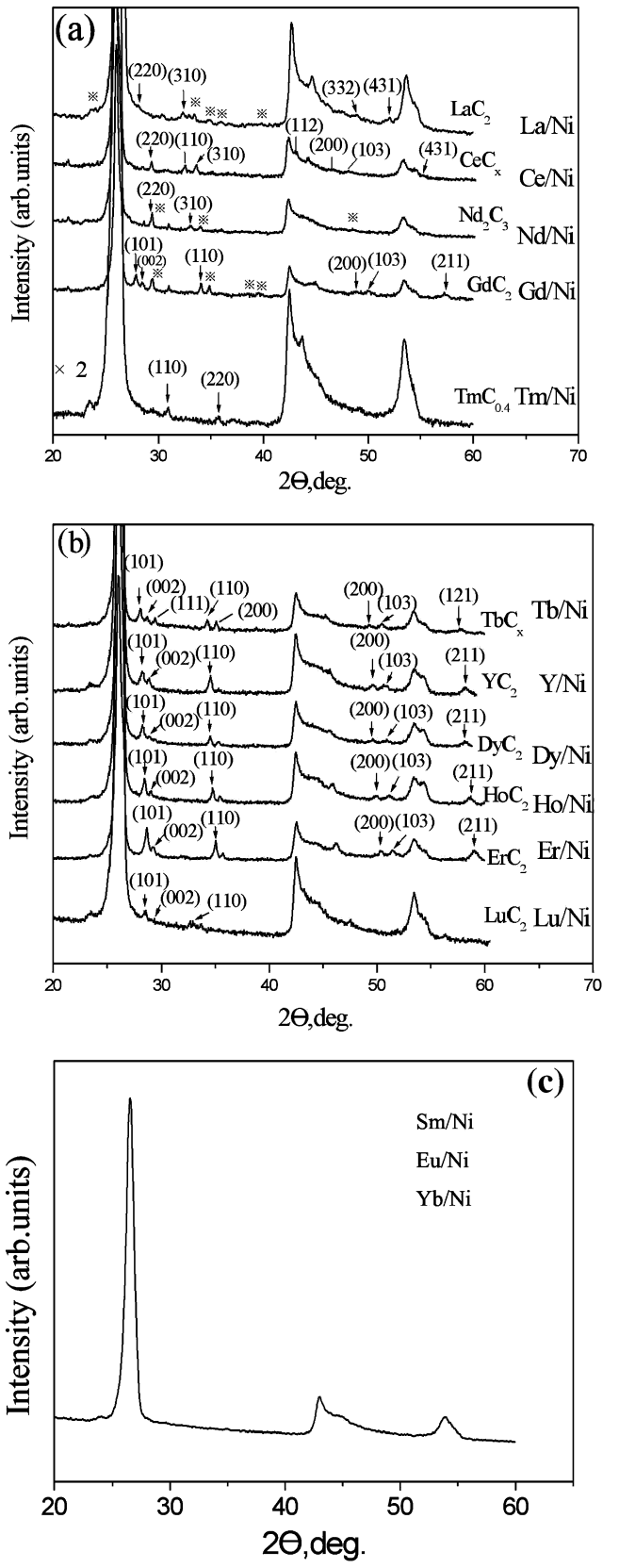


**Figure 5.** X-ray analysis of cathode deposits produced using RE/Ni catalysts based on (a) La, Ce, Nd, Gd, and Tm; (b) Tb, Y, Dy, Ho, Er, and Lu; and (c) Sm, Eu, and Yb.

catalyzing the formation of SWNTs is related to their very poor ability to form rare-earth carbides in an arc discharge. In addition, Tsui et al. observed experimentally that a stable carbide superlattice can be used as an ordered template of carbon-

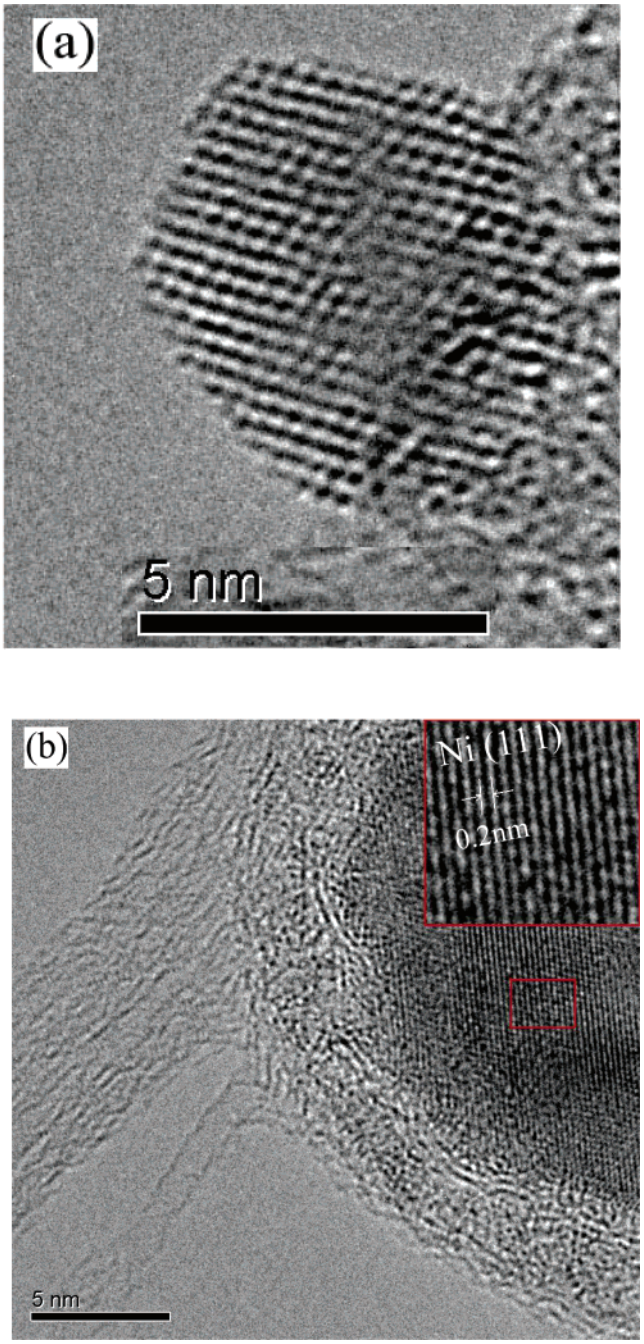


**Figure 6.** HRTEM images of a sample produced using the Eu/Ni catalyst: (a) $Eu_2O_3$ nanoparticle without wrap, (b) SWNT bundle associated with a catalyst particle. The inset shows a typical region of the particle containing pure metal Ni.

saturated "roots" for nucleating nanotube bundles.[18] A similar classification of a series of RE elements was also reported by Moro et al.[19] and Saito et al.[20] who studied metallofullerenes and encapsulation of rare-earth carbides, respectively, by arcing RE/C anodes. Therefore, these studies support our correlation between the ability of RE elements to form rare-earth carbides and their catalytic efficiency for the series of rare-earth metals.

To understand the huge differences within the series of RE metals in the formation of carbides in our experiments, we compared the properties of rare-earth metals in detail and found that the most likely factor is the $REC_2$ reaction temperature range for the series of RE metals (Table 1).[21] From this table, the temperature range of stability for rare-earth carbides from group A is clearly higher than that for europium, samarium, and

**TABLE 1: Electronic Configurations and Ionic Radii of the Studied Rare-Earth Elements and Their $REC_2$ Reaction Temperature Range**

| Ln | electronic configuration | ionic radius (pm) | $REC_2$ reaction temperature range (°C) |
|---|---|---|---|
| La | $5d6s^2$ | 106.1 | 1900−2600 |
| Ce | $4f^15d^16s^2$ | 103.4 | 1990−2300 |
| Nd | $4f^46s^2$ | 99.5 | 1670−2330 |
| Sm | $4f^66s^2$ | 96.4 | 1330−2050 |
| Eu | $4f^76s^2$ | 95 | 1200−1730 |
| Gd | $4f^75d^16s^2$ | 93.8 | 2000−2430 |
| Tb | $4f^96s^2$ | 92.3 | − |
| Dy | $4f^{10}6s^2$ | 90.8 | 2170−2590 |
| Ho | $4f^{11}6s^2$ | 89.4 | 1730−2560 |
| Er | $4f^{12}6s^2$ | 88.1 | 1755−2490 |
| Tm | $4f^{13}6s^2$ | 86.9 | 1500−2300 |
| Yb | $4f^{14}6s^2$ | 85.8 | 1100−1550 |
| Lu | $4f^{14}5d^16s^2$ | 85 | 2100−2600 |
| Y | $3d^14s^2$ | 88 | 2270−2550 |

ytterbium carbides. This indicates that group A rare-earth carbides are more stable than europium, samarium, and ytterbium carbides at higher temperatures, which agrees with our observations under the arc discharge conditions.

It is known that the greater the extent of the charge transfer, the easier the formation of metal−carbon clusters at high temperature. Moro et al.[19] supposed that the valence states of the RE metals encaged in metallofullerenes were responsible for the classification into groups, with a valence of 3+ for group A and 2+ for group B. This was confirmed by later studies.[22−24] Whereas most rare-earth elements in group A are trivalent and all group B RE elements have a tendency toward the 2+ oxidation state, the "intermediate performer" Tm has the lowest $Ln^{2+}/Ln^{3+}$ redox potential among the group B RE metals,[25] indicating that it has the greatest tendency of metals in this group to form the 3+ oxidation state. The different valence states of the RE metals are one of the most likely properties to cause the different abilities to form carbides under arc discharge conditions and, thus, to be correlated with the different catalytic efficiencies in the formation of SWNTs.

Very recently, a theoretical simulation of SWNT growth by a chemical vapor deposition (CVD) method suggested that the covalent bond formed between Fe and C is significantly stronger than that of Au−C, thus leading to the growth of SWNTs on an Fe catalyst but not on Au, for a given growth temperature.[26] These correlations further indicate that the interaction between the catalyst metal atoms and C atoms indeed plays a very important role in the formation of SWNTs regardless of the type of synthesis method employed. We also suggest that detailed simulations should be carried out to compare the behavior of group A and group B RE elements during SWNT growth to further understand how the abilities of RE to form carbides affect the formation of SWNTs.

## Summary

In summary, our studies show that the yield of SWNTs is greatly enhanced by the addition of a group A RE element to form a RE/Ni bimetallic catalyst, whereas addition of a group B RE element does not increase the yield of SWNTs. Among the group A RE metals, Tb/Ni, Er/Ni, Ho/Ni, and Y/Ni give the highest purity for the SWNTs formed. The huge difference between the two groups of RE elements in the yield of SWNTs was attributed to the different abilities of the rare-earth metals to form carbides. The results also indicate that the addition of different RE elements to Ni as catalysts affects the diameter distribution of the SWNTs produced. In the case of group A RE elements, the fraction of small-diameter tubes in the synthesized SWNTs samples decreases with decreasing ionic radius of the RE element. The diameter distribution of SWNTs produced using group A RE/Ni catalysts is different from that of group B RE/Ni catalysts, except for Tm.

**Acknowledgment.** This work was supported financially by (10144004, 10204010, 10574053), the Trans Century Training Programme Foundation for the Talents, RFDP (20020183050), the Cultivation Fund of the Key Scientific and Technical Innovation Project (2004-295) of MOE of China, the National Basic Research Program of China (2005 CB724400), and the Project for Scientific and Technical Development of Jilin Province and also by an exchange grant from the Swedish Research Council through the SIDA−Swedish Research Links exchange program.

## References and Notes

(1) *Carbon Nanotubes: Synthesis, Structure, Properties and Applications*; Dresselhaus, M. S., Dresselhaus, G., Avouris, P., Eds.; Springer: Berlin, 2001.

(2) Baughman, R. H.; Zakhidov, A. A.; de Heer, W. A. *Science* **2002**, *297*, 787.

(3) Kam, N. W.; Dai, H. *J. Am. Chem. Soc.* **2005**, *127*, 6021.

(4) Dresselhaus, M. S., Williams, K. A., Eklund, P. C. *MRS Bull.* **1999**, *24*, 45.

(5) Itkis, M. E.; Perea, D.; Niyogi, S.; Rickard, S.; Hamon, M.; Hu, H.; Zhao, B.; Haddon, R. C. *Nano Lett.* **2003**, *3*, 309.

(6) Journet, C.; Maser, W. K.; Bernier, P.; Loiseau, A.; Chapelle, M. L.; Lefrant, S.; Deniard, P.; Lee, R.; Fischer, J. E. *Nature* **1997**, *388*, 756.

(7) Liu, B.; Wågberg, T.; Olsson, E.; Yang, R.; Li, H.; Zhang, S.; Yang, H.; Zou, G.; Sundqvist, B. *Chem. Phys. Lett.* **2000**, *320*, 365.

(8) Shi, Z. J.; Okazaki, T.; Shimada, T.; Sugai, T.; Suenaga, K.; Shinohara, H. *J. Phys. Chem. B* **2003**, *107*, 2485.

(9) Yao, M. G.; Liu, B. B.; Zou, Y. G.; Wang, L.; Li, D. M.; Cui, T.; Zou, G. T.; Sundqvist, B. *Carbon* **2005**, *43*, 2894.

(10) Yudasaka, M.; Sensui, N.; Takizawa, M.; Bandow, S.; Ichihashi, T.; Iijima, S. *Chem. Phys. Lett.* **1999**, *312*, 155.

(11) Gavillet, J.; Thibault, J.; Stéphan, O.; Amara, H.; Loiseau, A.; Bichara, Ch.; Gaspard, J.-P.; Ducastelle, F. *J. Nanosci. Nanotechnol.* **2004**, *4*, 346.

(12) Krestinin, A. V.; Kislov, M. B.; Ryabenko, A. G. *J. Nanosci. Nanotechnol.* **2004**, *4*, 390.

(13) Deng, W. Q.; Xu, X.; William, A.; Goddard, III. *Nano. Lett.* **2004**, *4*, 2331.

(14) Rao, A. M.; Richter, E.; Bandow, S.; Chase, B.; Eklund, P. C.; Williams, K. A.; Fang, S.; Subbaswamy, K. R.; Menon, M.; Thess, A.; Smalley, R. E.; Dresselhaus, G.; Dresselhaus, M. S. *Science* **1997**, *275*, 187.

(15) Rao, A. M.; Chen, J.; Richter, E.; Schlecht, U.; Eklund, P. C.; Haddon, R. C.; Venkateswaran, U. D.; Kwon, Y. K.; Tomanek, D. *Phys. Rev. Lett.* **2001**, *86*, 3895.

(16) Liu, X.; Pichler, T.; Knupfer, M.; Golden, M. S.; Fink, J.; Kataura, H.; Achiba Y. *Phys. Rev. B* **2002**, *66*, 045411.

(17) Jost, O.; Gorbunov, A. A.; Pompe, W.; Pichler, T.; Friedlein, R.; Knupfer, M.; Reibold, M.; Bauer, H.-D.; Dunsch, L.; Golden, M. S.; Fink, J. *Appl. Phys. Lett.* **1999**, *75*, 2217.

(18) Tsui, F.; Ryan, P. A. *Phys. Rev. Lett.* **2002**, *89*, 15503.

(19) Moro, L.; Ruoff, R. S.; Becket, C. H.; Lorents, D. C.; Malhotra, R. *J. Phys. Chem.* **1993**, *97*, 6801.

(20) Saito, Y.; Okuda, M.; Yoshikawa, T. *J. Phys. Chem.* **1994**, *98*, 6696.

(21) Kosolapova, T. Y. *Handbook of High-Temperature Compounds*; Plenum Press: New York, 1990; pp 176−177.

(22) Iwasaki, K.; Wanita, N.; Hino, S.; Yoshimura, D.; Okazaki, T.; Shinohara, H. *Chem. Phys. Lett.* **2004**, *398*, 389.

(23) Sun, B. Y.; Inoue, T.; Shimada, T.; Okazaki, T.; Sugai, T.; Suenaga, K.; Shinohara, H. *J. Phys. Chem. B* **2004**, *108*, 9011.

(24) Shinohara, H. *Rep. Prog. Phys.* **2000**, *63*, 843.

(25) Qiang, S. *The Chemistry of Rare Earths*, 1st ed.; Zhengzhou: Henan, China, 1993; Chapter 1.

(26) Raty, J. Y.; Gygi, F.; Galli, G. *Phys. Rev. Lett.* **2005**, *95*, 96103.